İstanbul
GEDİK
University
2651-5199

International Journal of Engineering and Natural Sciences

IJENS's

Vol:2 - Issue:1 - Year : 2019

International Journal of Engineering and Natural Sciences (IJENS's), Vol. 2, Num. 1

Table of Contents:

Aim and Scope of IJENS's

International Journal of Engineering and Natural Sciences (IJENS) started its publishing life in December 2018. The aim of the journal is to serve researchers, engineers, scientists and all those who can benefit from it all over the world by providing theoretical and applicable knowledge in the field of engineering and natural sciences.

International Journal of Engineering and Natural Sciences (IJENS) covers a wide spectrum of research achievements. Thus, highly technological, creative and original research results, scientific reviews and short communication notes in a suitable balance of experimental, theoretical and computational aspects are considered for publication.

The publication language of the journal is English. Manuscripts previously published in another journal are not accepted.

The IJENS is free of charge and published three times a year. It allows authors to submit articles online and track their progress via its web interface.

Contact:

Istanbul Gedik University
Cumhuriyet Mahallesi İlkbahar Sokak No: 1-3-5
Yakacık 34876 Kartal, İstanbul, Turkey.
+90 - 216 444 5 438

International Journal of Engineering and Natural Sciences (IJENS's)
https://www.gedik.edu.tr/akademik-birimler/akademik-yayinlar/mf-dergisi
ijens@gedik.edu.tr

When looked at the magnitude and the impact of the scientific and technological advances over the last century, it is even more difficult to predict the scale of transformations that will take place in the future. The last 20 years saw foundational engineering disciplines such as Civil, Mechanical, Electrical, Industrial and Environmental marry Biology and Medicine, driving new interdisciplinary fields such as Biomechatronics, Life Sciences Engineering, Biomaterials, and Bioinformatics. Results of scientific research done anywhere in the world can now serve humanity as a whole, surpassing any borders.

Technological advances thrive when there are high levels and density of research and development activities. The higher the interaction between Natural Sciences (Mathematics, Physics, Chemistry) and Medicine and Biology, the higher the value of the end technology products, publications, and patents. Scientific research quality and value is demonstrated most significantly when the experiment and the theoretical approach of the research conducted is proven when it's well synthesized, and the end results are clearly shown to bring the scientific world novelty and inspiration.

With the goal of bringing the research conducted by Institutions and Science and Engineering Faculties of the universities closer to the researchers, and facilitating touch points amongst scientists, Istanbul Gedik University Engineering Faculty aims to publish the International Journal of Natural and Engineering Sciences (IJENS) three times every year. I am proud to introduce you to the new issue of this journal on behalf of my entire team.

Prof. Dr. Feriha ERFAN KUYUMCU

Editor

Analysis of the Model Predictive Current Control of the Two Level Three Phase Inverter

Çiğdem GÜNDOĞAN TÜRKER

Department of Mechatronic Engineering, Istanbul Gedik University
Istanbul, Turkey
cigdem.gundogan@gedik.edu.tr

Abstract: Model Predictive Control (MPC) Algorithms have been very popular and used widely in industrial applications of power converters and drives. Major advantage of MPC is the flexibility to control different variables, with constraints and additional system requirements. Also, it has been an alternative to the classical control techniques without need of additional modulation techniques, MPC needs the proper system model in order to calculate optimum values of the controlled variables. This paper gives an introduction about the Model Predictive Current Algorithm. Model Predictive Current Control Algorithm is implemented for a two phase three level drive system. After the system is modelled, the control algorithm is verified for different load condition of an induction machine.

Key Words: Two Level Three Phase Inverter, Induction Machine, Model Predictive Control.

1. INTRODUCTION

Predictive Control techniques have been applied in electrical machines and drive systems such as energy, communications, medicine, mining, transportation, etc. Most industrial applications such as automative, space and aeronautics, railway, ship transport, nuclear process have own particular requirements and need electrical drives with fault-tolerant and high reliability. With these requirements and growing voltage levels, the control of the multiphase converters has been improved in last ten years [1-2].

Field-oriented control (FOC) and direct torque control (DTC) methods are most established methods in three-phase electrical drives control. FOC is a modulation-based approach with a coordinate transformation from stator fixed to a rotor flux-oriented coordinate system. In DTC approach, the state of the switches is selected from a lookup table depending on the stator flux angle and the outputs of hysteresis controllers for flux and torque. As it is implied from the absence of a modulator, DTC shows a faster transient response than FOC but it has higher current, flux, and torque ripples [4-8].

Model Predictive Control (MPC) techniques with several advantages have been an alternative to conventional controllers. The common property of the Model Predictive Control Techniques is the precalculation of the future actions of the system in a prediction horizon time by using the system model directly. The optimal control action is defined according to a cost function. The system variables are been evaluated by comparing the reference values in a sampling time. The direct application of the control action to the converter without requiring a modulator is the main advantage of MPC. Also, the cost function is an important stage in the design of an MPC, since required constraints and nonlinearities of the multidimensional systems are easily implemented and evaluated to select the optimal switching states. However, the high switching frequency, current ripples and computational efforts are some major drawbacks [9-12].

This paper is organized as follows: Firstly, the whole system which includes induction machine driven by two level three phase inverter is described and modelled mathematically. In section 3, Model Predictive Control Algorithm is introduced detaily. Finally, the simulation of the control algorithm for the drive system is presented.

2. SYSTEM MODEL

In this study, the system is modelled for the induction machine driven by a two level three phase inverter. Two level three phase inverter topology and voltage vector are shown in Figure 1. Two semiconductor switches in each phase leg work in a complementary manner. When the upper switch is

on with switching state '1', the lower switch is off with switching state '0'. There are eight possible switching combinations for the two level three phase inverter as the variables $u_{abc} = [u_a \quad u_b \quad u_c]^T \in \{0,1\}$ are introduced. In this way, each phase of the two level inverter can produce two discrete voltage levels $-\frac{V_{dc}}{2}$ and $\frac{V_{dc}}{2}$ [13-14].

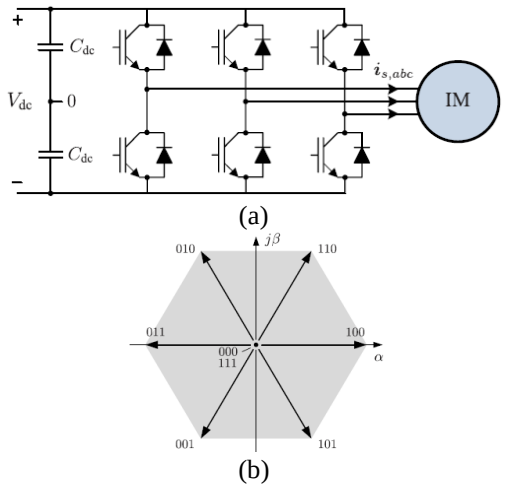

Figure 1. a) Topology of two level three phase inverter, b) Voltage vector diagram.

By employing the Clarke Transformation which the switching states are transformed from the abc plane to the $\alpha\beta$ plane, final control set contains only seven unique voltage vectors $v_{\alpha\beta} = [v_\alpha \quad v_\beta]^T$.

Thus, the actual voltages applied to the windings of the induction machine are calculated as;

$$v_{\alpha\beta} = \frac{V_{dc}}{2} u_{\alpha\beta} = \frac{V_{dc}}{2} K u_{abc} \tag{1}$$

The matrix K is given by;

$$K = \frac{2}{3}\begin{bmatrix} 1 & -1/2 & -1/2 \\ 0 & \sqrt{3}/2 & -\sqrt{3}/2 \end{bmatrix} \tag{2}$$

$[0 \quad 0 \quad 0]^T$ and $[1 \quad 1 \quad 1]^T$ produces zero voltage vectors called zero switching states, whereas the others produce active voltage vectors as active switching states.

Regarding the dynamics of the induction machine, the differential equations are given in $\alpha\beta$ coordinate system which is stator fixed for $\omega_k = 0$.

$$i_s + \tau_\sigma \frac{di_s}{dt} = \frac{1}{r_\sigma} \upsilon_s - j\omega_k \tau_\sigma i_s + \frac{k_r}{r_\sigma}\left(\frac{1}{\tau_r} - j\omega_{el}\right)\psi_r \tag{3}$$

$$\psi_r + \tau_r \frac{d\psi_r}{dt} = L_m i_s - j(\omega_k - \omega_{el})\tau_r \psi_r \tag{4}$$

Where the coefficients are given by $\tau_\sigma = \frac{\alpha L_s}{r_\sigma}$ and $r_\sigma = R_s + k_r^2 R_r$ with $k_r = \frac{L_m}{L_r}$, $\tau_r = \frac{L_r}{R_r}$ and $\sigma = 1 - \frac{L_m^2}{L_s L_r}$.

ψ_s, ψ_r ; the fluxes, i_s, i_r; the currents, R_s, R_r; the resistances, L_s, L_r; inductances, l_m; mutual inductance between stator and rotor, v_s; the stator voltage and v_r; the rotor voltage. $w_{el} = p * w_m$ is the electrical angular machine speed. $(*)_s$ denotes stator variables, $(*)_r$ denotes the rotor variables.

The stator flux ψ_s can be estimated as;

$$\frac{d\psi_s}{dt} = v_s - R_s i_s \tag{5}$$

The electromagnetic torque equation is given by;

$$T_e = \frac{3}{2} p(\psi_s \times i_s) = \frac{3}{2} p(\psi_r \times i_r) \tag{6}$$

The mechanical differential equation is can be described by

$$\frac{dw_m}{dt} = \frac{1}{j}(T_e - T_j) \tag{7}$$

3. MODEL PREDICTIVE CURRENT CONTROL

MPC needs the proper system model in order to calculate optimum values of the controlled variables. The system behaviour in next sampling interval is calculated for every switching state of the inverter in a certain prediction horizon. MPC determines the optimum switching states by minimizing a cost function. A cost function is defined according to the desired behavior of the system including controlled variables reference tracking by comparing the controlled variable with its reference value. Figure 2 shows the basic control scheme of the system [15].

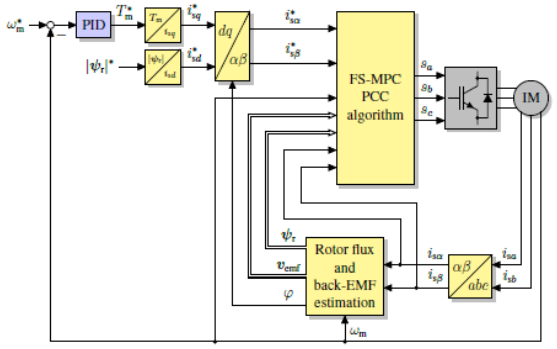

Figure 2. Basic control schema for the whole system

ISSN: 2651-5199

The predictive current controller relies on the model of the physical drive system to predict future stator current trajectories. The current references $i_{sd}^*$and i_{sq}^* are transformed to $\alpha\beta$ current references, $i_{s\alpha}^*$ and $i_{s\beta}^*$, and the controller operates in $\alpha\beta$ coordinates which makes the control more efficiently in stationary coordinates.

Conventional speed PID controller generates the torque reference. The constant reference value of the rotor flux magnitude is set. Based on the reference values of the field and torque, the currents i_{sd} and i_{sq} are produced by the equations below;

$$i_{sd}^* = \frac{|\psi_r|^*}{L_m} \tag{8}$$

$$i_{sq}^* = \frac{T^*}{\frac{3L_m}{2L_r}|\psi_r|^*} \tag{9}$$

The State-Space models of the induction machine can be designed as;

$$x=\begin{bmatrix} i_{s\alpha} \\ i_{s\beta} \\ \psi_{r\alpha} \\ \psi_{r\beta} \end{bmatrix}, \quad u=[\upsilon_\alpha,\upsilon_\beta], \quad y = i_s \tag{10}$$

y is taken as the system output vector, whereas $u_{\alpha\beta}$ constitutes the switching voltage vector provided by the controller.

❖ Based on the discrete model of system, the current values of the controlled variables (x(k)) at step k are used to predict their next values x(k+1) for all N possible switching states.

❖ In the proposed predictive algorithm, future current I(k+1) is evaluated for each of the possible seven voltage vectors which produce seven different current predictions.

❖ The voltage vector whose current prediction is closest to the expected current reference $x_{ref}(k+1)$ is applied to the load at the next sampling instant. In other words, the selected vector will be the one that minimizes the cost function.

Adding system constraints is a remarkable feature of MPC. These constraints can be added simply to the cost function with their specific weighting factors. It can be implemented by an additional term to the cost function as the distance between the measure value of voltage at the current state and the future state (one step time forward) as given below;

$$j=(i_{s\alpha}^*-i_s(k+1))^2+(i_{s\beta}^*-i_{s\beta}(k+1))^2+\lambda(u(k+1)-u(k))^2 \tag{11}$$

4. SIMULATION OF THE CONTROL ALGORITHM

MPC algorithm for the two level inverter and induction machine is simulated on the Matlab/Simulink in Figure 3. The algorithm is executed with a sampling time $T_s = 100\mu s$. The DC link voltage is 550V. The parameters of the induction machine is given in Table 1.

Table 1. The parameters of the induction machine.

Parameters	Value
Nominal power P_{nom}	$2.2kW$
Synchronous frequency f_{syn}	$50Hz$
Nominal current $\|i_{s,nom}\|$	$10A$
Nominal speed ω_{nom}	$2800rpm$
Number of pole pairs p	1
Stator resistance R_s	2.68Ω
Rotor resistance R_r	2.12Ω
Stator inductance L_s	$283.4mH$
Rotor inductance L_r	$283.4mH$
Mutual inductance L_m	$275.1mH$
Inertial J	$0.062kgm^2$

In the simulation, the reference value of the rotor flux magnitude is set to $|\psi_r|^* = 0.7Wb$. The torque reference is produced by the speed PI controller. The current references i_s^* are calculated as described in the MPC algorithm.

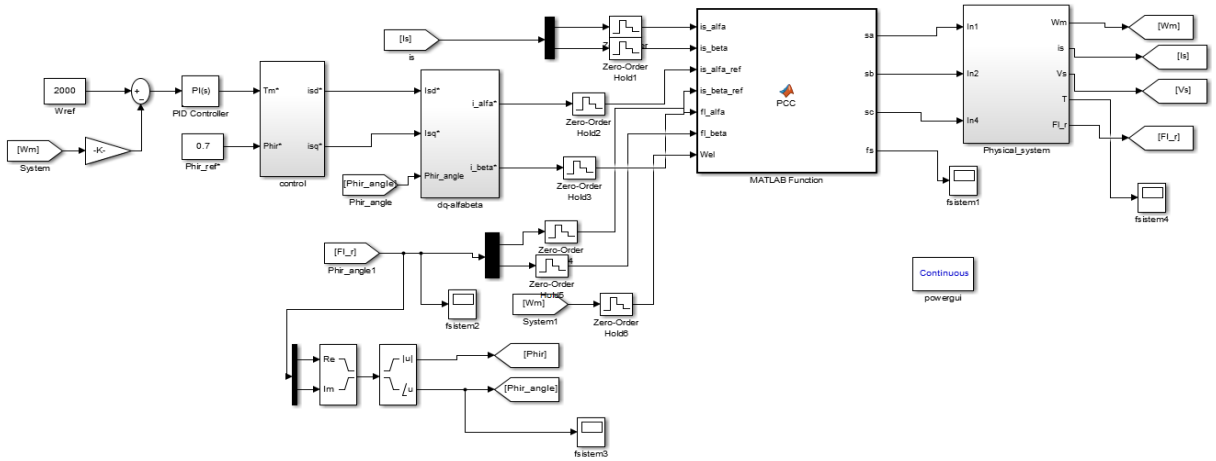

Figure 3. The simulation blocks of MPC of the two level inverter driving the induction machine.

The stator currents at 2800rpm without load torque are presented in Figure 4. Figure 5 shows the stator currents when a load torque of 4 Nm is implemented.

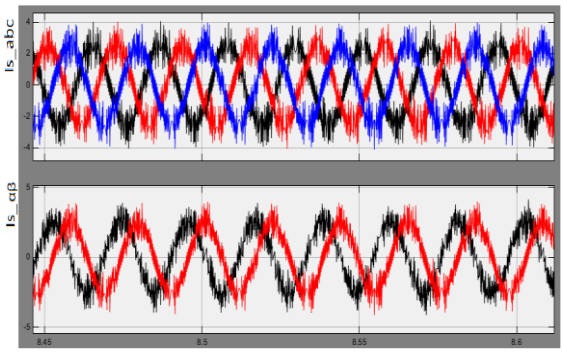

Figure 4. Steady state stator currents and αβ currents waveforms at no load and 2800rpm.

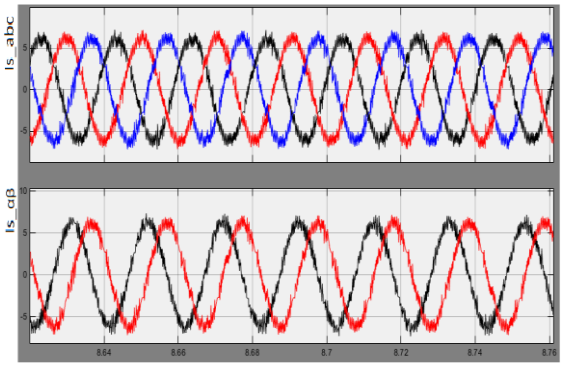

Figure 5. Steady state stator currents and αβ currents waveforms at 4Nm load torque and 2800rpm.

Figure 6 shows the load torque impact on the speed. At about time 7s, 4Nm was applied to the machine which was rotating at 2800rpm.

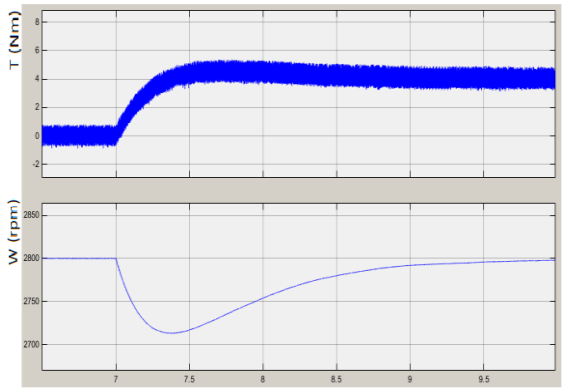

Figure 6. Load torque impact by changing from 0Nm to 4Nm at 2800rpm.

In Figure 7, speed reference impacts by changing from 1500 to 2800 rpm. Figure 8 shows the current control result by changing the speed reference.

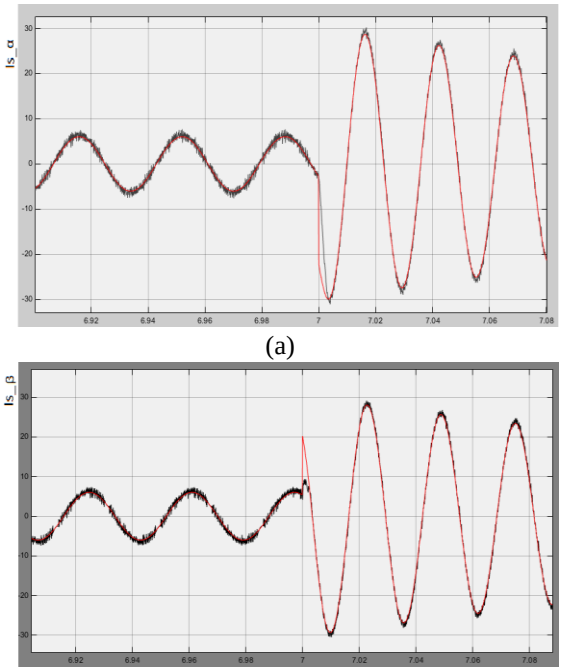

Figure 7. a) $I_{s\alpha}$ b) $I_{s\beta}$ stator current steps by changing the speed from 1500 to 2800 rpm.

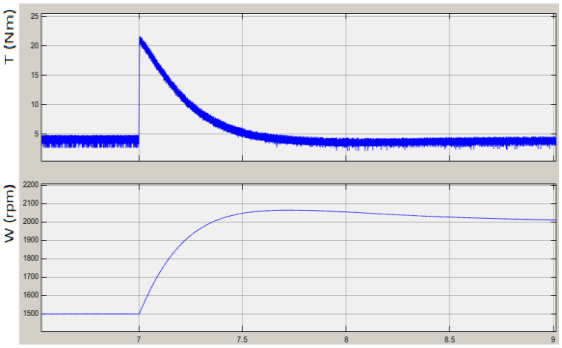

Figure 8. Speed reference impact, 4Nm at 2800 rpm.

5. CONCLUSION

Predictive control techniques have been a very powerful alternative in the electric drives applications. It is simple to apply and allows the control of different converters without the need of additional modulation techniques or internal cascade control loops. The important disadvantage of MPCs which is high calculation power is overcome by today's microcontrollers.

Major advantage of MPC is the flexibility to control different variables, with constraints and additional system requirements. This is great potential and flexibility to improve the performance, efficiency, and safety demanded by the industry applications.

Model Predictive Current Control is introduced and presented for the system consisting of a two level inverter and an induction machine. It is

ISSN: 2651-5199

implemented in Matlab/Simulink and obtained simulation results of the system for different load and speed conditions. It is clearly seen that the algorithms can track the system references without any problems for steady state and speed steps.

REFERENCES

1. Morari, M., Lee, J.H., 1999. Model predictive control: past,present and future, Comp.Chem.Eng., 23, p.667-682.
2. Lee, J.H., 2011. Model Predictive Control: Review of the three decades of development, Int.J.Cont.Autom.Syst, 9(3), p. 415-424.
3. Linder, A., Kennel R., "Model Predictive Control for Electric Drives", 36th Power Electronics Specialists Conference, 2005, 1793-1799.
4. Kazmierkowski M.P., Krishnan R., ve Blaabjerg, "Control in Power electronics, NewYork:Academic Press, 2002.
5. Wang F., Li S., Mei X., Xie W., Rodriguez J., Kennel, R.M.,"Model-Based Predictive Direct Control Strategies for Electrical Drives: An Experimental Evaluation of PTC and PCC Methods", IEEE Trans. On Ind. Informations, 11,3, 2015.
6. Cortes,P.,Kazmierkowski, M.P., Kennel, R.M., Quevedo, D.E. ve Rodriguez, J., "Predictive Control in Power Electronics and Drives", *IEEE Trans. Ind. Electron.*, 55, 12, 4312-4324, Dec.2008.
7. Kennel, R., Rodriguez, J., Espinoza, J., Trincado, M., 2010. High Performance Speed Control Methods for Electrical Machines: An Assessment, IEEE Int. Conf. On Industrial Technology, p.1793-1799.
8. Buja, G.S., Kazmierkowski, M.P., Direct Torque Control of PWM Inverter-Fed AC motors- a Survey, IEEE Trans. on Industial Electronics.,1793-1799.
9. Geyer, T., Papafotiou, G. And Morari, M., "Model Predictive Direct Torque Control-Part1: Concept, algorithm and Analsis", IEEE Trans. Ind. Electron, 56, 6, 2009, 1894-1905.
10. Papafotiou, G., Kley, J., Papadopolus, K.G., Bohnen, P., and Morari, M., "Model Predictive Direct Torque Control –Part II: Implementation and Experimental Evaluation", IEEE Trans. Ind. Electron, 56, 6, 2009, 1906-1915
11. Geyer, T., 2014. Quevedo, D.E., "Multistep Finite Control Set Model Predictive Control for Power Electronics", IEE Trans. On Power Electronics, 29, 12.
12. Scoltock, J., Geyer, T., Madawana, U., 2013. A Comparison of Model Predictive Control Schemes for MV Induction Motor Drives, IEEE Trans.of Industrial Informatics, 9(2), p.909-919.
13. Rodríguez J., Pontt J., Silva C., Correa P., Lezana P., Cortes P., Amman U., "Predictive Current Control of a Voltage Source Inverter IEEE Trans. On Industrial Electronics, 54, 1, February 2007.
14. Karamanakos, P., Stolze P., Kennel R.M., Manias S., Mouton H.T., "Variable Switching Point Predictive Torque Control of Induction Machines", *IEEE Journal of Emerging and Selected Topics in Power Electronics*, 2,2, 2014.
15. Stolze, P., Karamanakos, P., Moiton, T., Manias, S.N., 2013. Heuristic Variable Switching Point Predictive Current Control for the Three-Level Neutral Point Clamped Inverter", SLED.

Spouted Bed Drying Characteristics of Rosehip (Rosa Canina L.)

Duygu Evin

Department of Mechanical Engineering, Firat University
Elazig, Turkey
devin@firat.edu.tr

Abstract: Drying kinetics, effective moisture diffusivity and activation energy of rosehip (Rosa Canina L.) dried in a spouted bed dryer were investigated. The effects of the spouted bed drying and the inlet air temperature in the range of 40-80°C on the moisture ratio degradation and the drying rate of rosehip (Rosa Canina L.) were studied experimentally. Drying took place in the falling rate period. Drying time was reduced by 83% using a temperature of 80°C instead of 40°C. The effective moisture diffusivities of rosehip under spouted bed drying ranged from 2.5x10-10 to 2.56 x10-9 m2/s. The values of diffusivities increased with the increase in inlet air temperature. An Arrhenius relation with an activation energy value of 51.6 kJ/mol expressed the effect of temperature on the diffusivity.

Keywords: Spouted bed drying; rosehip; drying kinetics; effective moisture diffusivity; activation energy.

1. INTRODUCTION

In recent years, much attention has been paid to the quality of foods during drying. Both the method of drying and physicochemical changes that occur during drying affects the quality of the dehydrated product [1]. Since rosehip fruits are rich source of vitamin C and also have a rich composition (K, P minerals and vitamin contents), they have traditionally been used as a vitamin supplement or for health food products in many European countries. Rosehip extracts also possess high antioxidant capacity as well as antimutagenic effects [2].

Spouted bed technology in solid-gas system [3] has been proven to be an effective means of contacting for gas and course solid particles such as Geldart type D particles [4]. Since the agitation of solids which permits the use of high air temperature provides rapid drying without the risk of thermal damage, drying of coarse, heat sensitive granular materials has been the most popular application of the spouted beds.

In present study, drying kinetics, effective moisture diffusivity, and activation energy of rosehips dried in the spouted bed dryer were investigated. The effects of the spouted bed drying, the inlet air temperature and the initial moisture content of the rosehips on the investigated properties were discussed.

2. MATERIAL AND METHOD

2.1. Samples

Fresh rosehips (Rosa Canina L.) were harvested by hand. They were collected in different months (September and October) because it was also aimed to investigate the effect of the initial moisture content of the rosehips on drying. Rosehips approximately the same size were selected and the average length and the diameter were measured as 2.02 and 1.125 cm, respectively. An infrared moisture analyzer (Sartorius MA45, Germany) was used to determine the initial moisture contents.

2.2. Drying procedure

The experimental set-up of Paraboloid Based Spouted Bed (PBSB) dryer and the spouted bed drying mechanism are given in Fig.1 and Fig.2, respectively. The details of the experimental set-up and the spouted bed drying procedure were given in a previous study of the author [5].

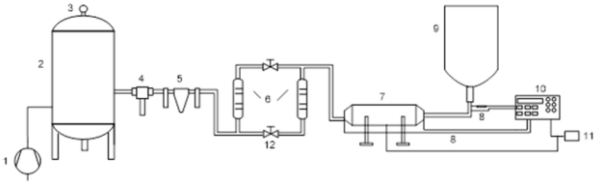

Figure 1. (1) Screw type compressor, (2) Air tank, (3) Pressure gauge, (4) Air filter, (5) Pressure regulator, (6) Rotameters, (7) Electric heater, (8) T type thermocouples,

(9) Spouted bed, (10) Data acquisition board, (11) PID controller.

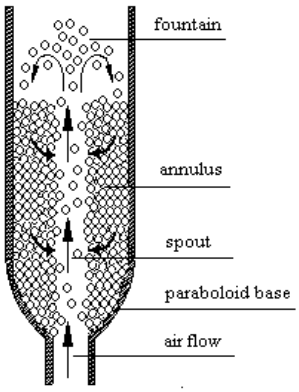

Figure 2. The spouted bed drying mechanism.

1.5 kg of rosehips were dried at 40, 70 and 80oC inlet air temperatures with 85 m3/h air flow rate. At ten minute intervals, rosehip samples (approximately 5 g) were removed from the spouted bed. The moisture content of the samples during drying was determined with an infrared moisture analyzer (Sartorius MA45) to obtain the variation of moisture content with drying time.

2.3. Effective moisture diffusivity

The experimental drying data for determination of diffusivity was interpreted by using Fick's second law.

$$\frac{\partial M}{\partial t} = D_{eff}\frac{\partial^2 M}{\partial r^2} \quad (1)$$

The solution to Eq. (1) developed by Crank (1975) [6] can be used for various regularly shaped bodies. Assuming uniform initial moisture distribution, constant diffusion coefficient and negligible shrinkage Eq. (2) can be applicable for particles with cylindrical geometry.

$$MR = \frac{4}{\pi^2}\exp\left(-\pi^2\frac{D_{eff}\,t}{r^2}\right) \quad (2)$$

where MR is the moisture ratio and Deff is the effective moisture diffusivity, m^2/s.

2.4. Activation energy

The factors affecting Deff are significant to clarify the drying characteristics of a food product. Temperature is one of the strongest factor that effects on Deff. This effect can generally be described by an Arrhenius equation [9]:

$$D_{eff} = D_0\exp\left(-10^3\frac{E_a}{\bar{R}\,T}\right) \quad (3)$$

where, D_0 is the Arrhenius factor (m2/s), E_a is the activation energy for diffusion (kJ/mol), R¯is the universal gas constant (kJ/mol.K), and T is the air temperature (K).

3. RESULTS AND DISCUSSION

3.1. Drying Kinetics

The spouted bed drying curve of rosehip in which the moisture content decreases with the drying time is given in Fig 3. The effect of the air temperature on drying of rosehips can also be seen in this figure. Moisture content decreases gradually at 40°C. On the other hand, there is a sharp decrease in moisture content at 80°C. The drying time required for reducing the moisture content of rosehip from 0.44 to 0.07 (g water/g dry matter) changed between 1035 and 180 min depending on the air temperature. Increasing the air temperature in a certain air temperature range (40-80°C in this study) accelerates the drying process.

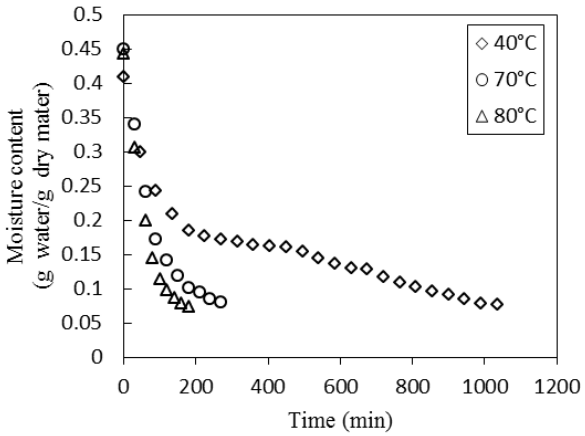

Figure 3. The spouted bed drying curve of rosehip.

The variation of drying rate with moisture ratio which explains the spouted bed drying behavior of rosehip is represented by Fig. 4. The curve shows only the falling rate period. In spouted bed drying, the whole surface of the solid is in contact with the air, so high heat and mass transfer coefficients cause a rapid evaporation at the surface. Therefore, main drying takes part in the spout region. However, moisture needs time to be transferred from the inner part of the solid to the surface. This especially occurs in the falling rate period at which the internal diffusion is essential. In the annulus region of the spouted bed, the moisture distribution of the particles are homogenized while traveling from the top to the bottom. As can be seen from this figure, drying rate increased with the increasing air temperature. The highest drying rates were achieved for spouted bed drying at 80oC inlet air temperature.

Effect of the initial moisture content on spouted bed drying of rosehip and variation of the drying rate for 0.44 and 0.8 initial moisture contents are represented in Fig. 5 and Fig. 6, respectively. So as to investigate the effects of initial moisture ratio on drying kinetics, a group of rosehips were harvested in September and the other in October.

ISSN: 2651-5199

Therefore rosehips with two different initial moisture contents (Mo) 0.44 and 0.80 (g water/ g dry matter) were dried in the spouted bed. Increase in the initial moisture content from 0.44 to 0.80 db increased the drying time by 55%.

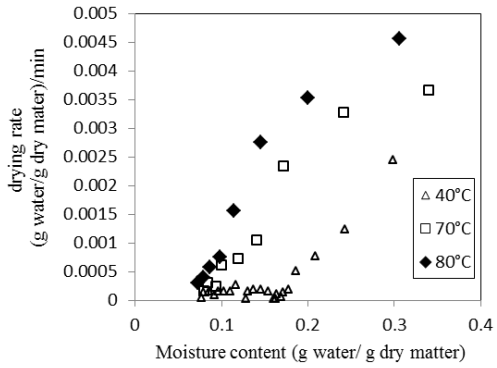

Figure 4. The variation of drying rate with moisture ratio.

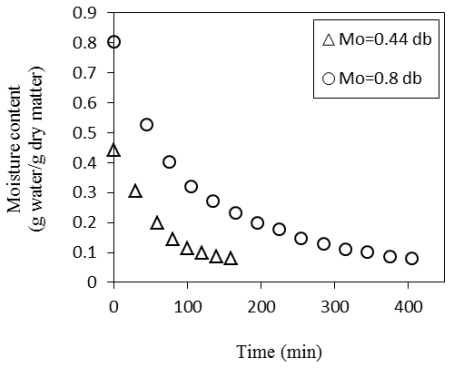

Figure 5. Effect of the initial moisture content on spouted bed drying of rosehip and variation of the drying rate for 0.44 and 0.8 initial moisture contents.

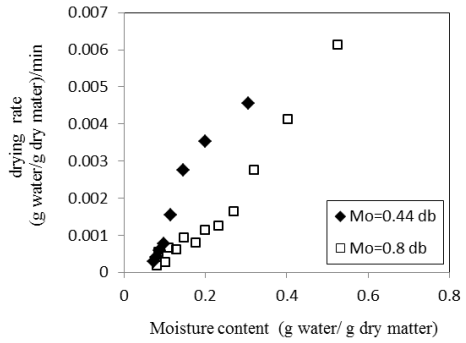

Figure 6. Effect of the initial moisture content on spouted bed drying of rosehip and variation of the drying rate for 0.44 and 0.8 initial moisture contents.

3.2. Effective moisture diffusivity and activation energy

Values of the effective moisture diffusivities of rosehip determined by Eq.7 are given in Table 2. The effective diffusivities of rosehip under spouted bed drying at 40-80oC ranged from 2.5x10-10 to 2.56 x10-9 m2/s. The values of diffusivities increased with the increase in inlet air temperature. The determined values lie within the general range of 10-11 to 10-9 m2/s for food materials [10].

Fig.7 shows the influence of temperature on the effective diffusivity. The values of ln(Deff) plotted versus 1/T was found to be essentially a straight line in the range of temperatures indicating Arrhenius dependence.

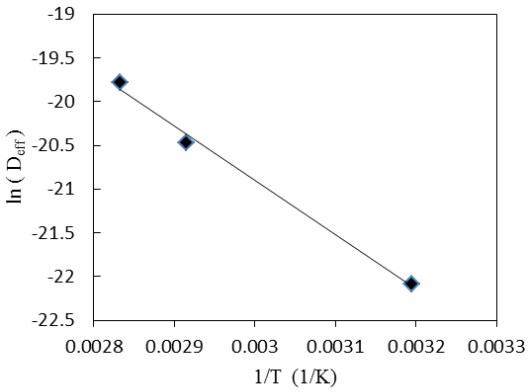

Figure 7. The influence of temperature on the effective diffusivity.

The activation energy of rosehip was found to be 51.6 kJ/mol. This activation energy for water diffusion in rosehip is higher than those given in the literature for convective drying of other foods such as; red chilli, 37.76 kJ/mol [11]; potato, 12.32-24.27 kJ/mol [12]; green bean, 35.43 kJ/mol [13]; carrot 28.36 kJ/mol [14], and pistachio nuts, 30.79 [15], but lower than mint 82.93 kJ/mol [16] and coconut 81.11 kJ/mol [17].

4. CONCLUSION

Drying took place in the falling rate period. Increasing the air temperature in a certain air temperature range (40-80oC in this study) accelerated the drying process. Drying time was reduced by 83% using a temperature of 80°C instead of 40°C. The effective diffusivities of rosehip under spouted bed drying at 40-80oC ranged from 2.5x10-10 to 2.56 x10-9 m2/s. The values of diffusivities increased with the increase in inlet air temperature. The activation energy of rosehip was found to be 51.6 kJ/mol. Increase in the initial moisture content from 0.44 to 0.80 db increased the drying time by 55%.

ACKNOWLEDGMENT

Financial support from the Scientific and Technological Research Council of Turkey (TUBITAK Project number: 104M346) is gratefully acknowledged.

REFERENCES

[1] Koyuncu, T., Tosun, I. & Ustun, N. S. (2003). Drying Kinetics and Color Retention of Dehydrated Rosehips. Drying technology, 21(7), 1369–1381.

[2] Erenturk, S., Gulaboglu, M. S. & Gultekin, S. (2005). The effects of cutting and drying medium on the vitamin C content of rosehip during drying. Journal of Food Engineering, 68, 513–518.

[3] Mathur, K.B. & Epstein, N. (1974). Spouted Beds. Academic Press, New York.

[4] Geldart, D. (1986). Gas fluidization technology. Wiley, New York.

[5] Evin, D., Gul, H. & Tanyıldızı, V. (2008). Grain drying in a paraboloid-based spouted bed with and without draft tube. Drying Technology, 26, 1577–1583.

[6] Crank, J. The mathematics of diffusion. Oxford, UK: Oxford University press (1975).

[7] Babalis S.J., Belessiotis V.G., Influence of the drying conditions on the drying constants and moisture diffusivity during the thin-layer drying of figs. Journal of Food Engineering 65 (2004) 449–458

[8] Togrul, H. Suitable drying model for infrared drying of carrot. Journal of Food Engineering 77 (2006) 610–619

[9] Henderson, S.M. (1974). Progress in developing the thin layer drying equation. Trans. ASAE. 17:1167-1172.

[10] Erbay Z., Icier F. (2010). A Review of Thin Layer Drying of Foods: Theory, Modeling, and Experimental Results. Critical Reviews in Food Science and Nutrition, 50:441–464.

[11] Kaleemullah, S., Kailappan, R. (2006). Modelling of thin layer drying kinetics of red chillies. Journal of Food Engineering. 76:531-537.

[12] Senadeera, W., Bhandari, B.R., Young, G., Wijesinghe, B. (2003). Influence of shapes of selected vegetable materials on drying kinetics during fluidized bed drying. Journal of Food Engineering. 58, 277-283.

[13] Doymaz, I. (2005). Drying behavior of green beans. Journal of Food Engineering. 69:161-165.

[14] Doymaz, I. (2004). Convective air drying characteristics of thin layer carrots. Journal of Food Engineering. 61:359-364.

[15] Kashaninejad, M., Mortazavi, A., Safekordi, A., Tabil, L.G. (2007). Thin-layer drying characteristics and modeling of pistachio nuts. Journal of Food Engineering. 78:98-108.

[16] Park, K.J., Vohnikova, Z., Brod, F.P.R. (2002). Evaluation of drying parameters and desorption isotherms of garden mint leaves (Mentha crispa L.). Journal of Food Engineering. 51:193-199.

[17] Madamba, P.S. (2003). Thin layer drying models for osmotically pre-dried young coconut. Drying Technology, 21:1759-1780.

 ISSN: 2651-5199

Some Curvature Properties of Generalized Complex Space Forms

Pegah Mutlu

Faculty of Engineering, Istanbul Gedik University
Kartal, 34876, Istanbul, Turkey
pegah.mutlu@gedik.edu.tr

Abstract: The object of the present paper is to study generalized complex space forms satisfying curvature identities named Walker type identities. Also It is proved that the difference tensor $R.\widetilde{C} - \widetilde{C}.R$ and the Tachibana tensor $Q(S, \widetilde{C})$ of any generalized complex space form $M(f_1, f_2)$ of dimensional $m \geq 4$ are linearly dependent at every point of $M(f_1, f_2)$. Finally generalized complex space forms are studied under the condition $R.R - Q(S,R) = L\, Q(g, \widetilde{C})$.

Keywords: Generalized complex space forms, Conharmonic curvature tensor, Walker type identity, Pseudosymmetric manifold, Tachibana Tensor.

1. INTRODUCTION

In 1989, Z. Olszak has worked on the existence of a generalized complex space form [1]. In [2], U.C. De and A. Sarkar studied the nature of a generalized Sasakian space form under some conditions regarding projective curvature tensor. They also studied Sasakian space forms with vanishing quasi-conformal curvature tensor and investigated quasi-conformal flat generalized Sasakian space forms, Ricci-symmetric and Ricci semisymmetric generalized Sasakian space forms [3]. Venkatesha and B.Sumangala [4], M. Atceken [5], S. Yadav and A. K. Srivastava [6] studied on generalized space form satisfying certain conditions on an M-projective curvature tensor, concircular curvature and psedo projective curvature tensor $\widetilde{P}$ satisfying $R.\widetilde{P} = 0$ and many authors studied on generalized Sasakian space form [7]. M.C. Bharathi and C. S. Bagewadi [8] extended the study to W_2 curvature, conharmonic and concircular curvature tensors on generalized complex space forms.

Motivated by these ideas, in the present paper, we study generalized complex space forms satisfying curvature identities named Walker type identities. The difference tensor $R.\widetilde{C} - \widetilde{C}.R$ and the Tachibana tensor $Q(S, \widetilde{C})$ of any generalized complex space form $M(f_1, f_2)$ of dimensional $m \geq 4$ are linearly dependent at every point of $M(f_1, f_2)$. Generalized complex space forms are studied under the condition $R.R - Q(S,R) = L\, Q(g, \widetilde{C})$.

A Kaehler manifold is an even dimensional manifold M^m, where $m=2n$ with a complex structure J and a positive definite metric g which satisfies the following conditions [9]

$$J^2 = -I, \quad g(JX, JY) = g(X, Y) \quad \text{and} \quad \nabla J = 0,$$

where ∇ denotes the covariant derivative with respect to Levi-Civita connection.

Let (M, J, g) be a Kaehler manifold with constant holomorphic sectional curvature $K(X \wedge JX) = c$, then is said to be a complex space form and it is well known that its curvature tensor satisfies the equation

$$R(X,Y)Z = \frac{c}{4}\{g(Y, Z)X - g(X, Z)Y + g(X,JZ)JY - g(Y, JZ)JX + 2g(X, JY)JZ\}, \quad (1)$$

for any vector fields X ,Y, Z on M.

An almost Hermitian manifold M is called a generalized complex space form $M(f_1, f_2)$ if its Riemannian curvature tensor R satisfies

$$R(X,Y)Z = f_1\{g(Y, Z)X - g(X, Z)Y\} + f_2\{g(X, JZ)JY - g(Y, JZ)JX + 2g(X, JY)JZ\}, \quad (2)$$

for any vector fields $X,Y,Z \in TM$, where f_1 and f_2 are smooth functions on M [10,11].

For a generalized complex space form $M(f_1, f_2)$ we have

$$S(X, Y) = \{(m-1)f_1 + 3f_2\}g(X, Y), \quad (3)$$
$$QX = \{(m-1)f_1 + 3f_2\}X, \quad (4)$$
$$r = m\{(m-1)f_1 + 3f_2\}, \quad (5)$$

where S is the Ricci tensor, Q is the Ricci operator and r is the scalar curvature of $M(f_1, f_2)$.

2. PRELIMINARIES

In this section, we recall some definitions and basic formulas which will be used in the following sections.

Let (M, g) be an n-dimensional, $n \geq 3$, semi-Riemannian connected manifold of class $\mathcal{C}^{\infty}$ with Levi-Civita connection ∇ and $\Xi(M)$ being the Lie algebra of vector fields on M.

We define on M the endomorphisms $X \bigwedge_A Y$, $\mathcal{R}(X,Y)$ and $\widetilde{\mathcal{C}}(X,Y)$ of $\Xi(M)$ by

$$(X \bigwedge_A Y)Z = A(Y,Z)X - A(X,Z)Y, \tag{6}$$

$$\mathcal{R}(X,Y)Z = \nabla_X \nabla_Y Z - \nabla_Y \nabla_X Z - \nabla_{[X,Y]} Z, \tag{7}$$

$$\widetilde{\mathcal{C}}(X,Y)Z = \mathcal{R}(X,Y)Z - \frac{1}{n-2}[X \bigwedge_g QY - Y \bigwedge_g QX]Z, \tag{8}$$

respectively, where A is a symmetric (0,2)-tensor on M and $X,Y,Z \in \Xi(M)$. The Ricci tensor S, the Ricci operator Q and the scalar curvature r of (M, g) are defined by $S(X,Y) = tr\{Z \to \mathcal{R}(Z,X)Y\}$, $g(QX,Y) = S(X,Y)$ and $r = tr\,Q$, respectively. [X,Y] is the Lie bracket of vector fields X and Y. In particular we have $(X \bigwedge_g Y) = X \bigwedge Y$.

The Riemannian-Christoffel curvature tensor R, the conharmonic curvature tensor $\tilde{C}$ and the (0,4)-tensor G of (M, g) are defined by

$$R(X_1, X_2, X_3, X_4) = g(\mathcal{R}(X_1, X_2)X_3, X_4),$$
$$\widetilde{\mathcal{C}}(X_1, X_2, X_3, X_4) = g(\widetilde{\mathcal{C}}(X_1, X_2)X_3, X_4),$$
$$G(X_1, X_2, X_3, X_4) = g((X_1 \bigwedge_g X_2)X_3, X_4),$$

respectively, where $X_1, X_2, X_3, X_4 \in \Xi(M)$.

From (8) it follows that

$$\widetilde{C}(X,Y,Z,W) = -\widetilde{C}(Y,X,Z,W),$$
$$\widetilde{C}(X,Y,Z,W) = -\widetilde{C}(X,Y,W,Z),$$
$$\widetilde{C}(X,Y,Z,W) = \widetilde{C}(Z,W,X,Y),$$
$$\widetilde{C}(X,Y,Z,W) + \widetilde{C}(X,,Z,W,Y) + \widetilde{C}(X,W,Y,Z) = 0.$$

Let $\mathcal{B}(X,Y)$ be a skew-symmetric endomorphism of $\Xi(M)$. We define the (0,4)-tensor B by $B(X_1,X_2,X_3,X_4) = g(\mathcal{B}(X_1,X_2)X_3, X_4)$. The tensor B is said to be a generalized curvature tensor if

$$B(X_1, X_2, X_3, X_4) = B(X_3, X_4, X_1, X_2),$$
$$B(X_1, X_2, X_3, X_4) + B(X_2, X_3, X_1, X_4) + B(X_3, X_1, X_2, X_4) = 0.$$

For a (0,k)-tensor field T, $k \geq 1$, a symmetric (0,2)- tensor field A and a generalized curvature tensor B on (M , g), we define the (0, k+2)-tensor fields B .T and Q(A, T) by

$$(B.T)(X_1, ..., X_k; X, Y) = -T(\mathcal{B}(X, Y)X_1, X_2, ..., X_k) - \cdots - T(X_1, X_2, \ldots, X_{K-1}, \mathcal{B}(X,Y)X_k),$$

$$Q(A,T)(X_1, ..., X_k; X, Y) = -T((X \bigwedge_A Y)X_1, X_2, ..., X_k) - \cdots - T(X_1, X_2, \ldots, X_{K-1}, (X \bigwedge_A Y)X_k),$$

respectively, where $X, Y, Z, X_1, X_2, ..., X_k \in \Xi(M)$.

Let (M, g) be covered by a system of charts $\{W; x^k\}$. We define by g_{ij} , R_{hijk} , S_{ij} , and

$$\widetilde{C}_{hijk} = R_{hijk} - \frac{1}{n-2}(g_{hk}S_{ij} - g_{hj}S_{ik} + g_{ij}S_{hk} - g_{ik}S_{hj}), \tag{9}$$

the local components of the metric tensor g, the Riemannian-Christoffel curvature tensor R, the Ricci tensor S, and the conharmonic curvature tensor $\widetilde{C}$, respectively.

Further, we denote by $S_{ij} = S_{ir}g^r_j$ and $S^j_i = g^{jr}S_{ir}$.

The local components of the (0, 6)-tensor fields R.T and Q (g ,T) on M are given by

$$(R.T)_{hijklm} = -g^{rs}(T_{rijk}R_{shlm} + T_{hrjk}R_{silm} + T_{hirk}R_{sjlm} + T_{hijr}R_{sklm}), \tag{10}$$

$$Q(g,T)_{hijklm} = -g_{mh}T_{lijk} - g_{mi}T_{hljk} - g_{mj}T_{hilk} - g_{mk}T_{hijl} + g_{lh}T_{mijk} + g_{li}T_{hmjk} + g_{lj}T_{himk} + g_{lk}T_{hijm}, \tag{11}$$

where T_{hijk} are the local components of the tensor T.

In this part we present some considerations leading to the definition of Deszcz Symmetric (Pseudosymmetric in the sense of Deszcz) and Ricci-pseudosymmetric manifolds.

A semi-Riemannian manifold (M,g) satisfying the condition $\nabla R = 0$ is said to be locally symmetric. Locally symmetric manifolds form a subclass of the class of manifolds characterized by the condition

$$R.R = 0 \tag{12}$$

where R. R is a (0,6)-tensor field with the local components

$$(R.R)_{hijklm} = \nabla_m\nabla_l R_{hijk} - \nabla_l\nabla_m R_{hijk} = g^{rs}(R_{rijk}R_{shlm} + R_{hrjk}R_{silm} + R_{hirk}R_{sjlm} + R_{hijr}R_{sklm}).$$

Semi-Riemannian manifolds fulfilling (12) are called semisymmetric [12]. They are not locally symmetric, in general.

A more general class of manifolds than the class of semisymmetric manifolds is the class of pseudosymmetric manifolds.

A semi-Riemannian manifold (M,g) is said to be pseudosymmetric in the sense of Deszcz [13,14] if at every point of M the condition

$$R.R = L_R Q(g,R) \tag{13}$$

holds on the set $\mathcal{U}_R = \left\{x \in M \,\middle|\, R - \frac{r}{n(n-1)}G \neq 0 \text{ at } x\right\}$, where L_R is some function on $\mathcal{U}_R$.

A semi-Riemannian manifold (M, g) is said to be Ricci-pseudosymmetric [15] if at every point of M the condition

$$R.S = L_s Q(g,S) \tag{14}$$

ISSN: 2651-5199

holds on the set $\mathcal{U}_s = \left\{x \in M \left| S - \frac{r}{n} g \neq 0 \text{ at } x \right.\right\}$, where L_s is some function on $\mathcal{U}_s$. Every pseudosymmetric manifold is Ricci-pseudosymmetric. The converse statement is not true. The class of Ricci-pseudosymmetric manifolds is an extension of the class of Ricci-semisymmetric (R.S= 0) manifolds as well as of the class of pseudosymmetric manifolds. Evidently, every Ricci-semisymmetric is Ricci-pseudosymmetric. There exist various examples of Ricci-pseudosymmetric manifolds which are not pseudosymmetric.
(13), (14) or other conditions of this kind are called curvature conditions of pseudosymmetry type [16].

3. WALKER TYPE IDENTITIES ON GENERALIZED COMPLEX SPACE FORMS

In this section, we present results on generalized complex space forms satisfying curvature identities named Walker type identities.

LEMMA 3.1 [17]. *For a symmetric (0,2)-tensor A and a generalized curvature tensor $\mathcal{B}$ on a semi-Riemannian manifold (M,g), n ≥ 3, we have*

$$\sum_{(X_1,X_2)(X_3,X_4)(X,Y)} Q(A, \mathcal{B})(X_1, X_2, X_3, X_4; X, Y) = 0. \qquad (15)$$

It is well-known that the following identity

$$\sum_{(X_1,X_2)(X_3,X_4)(X,Y)} (R \cdot R)(X_1, X_2, X_3, X_4; X, Y) = 0 \qquad (16)$$

holds on any semi-Riemannian manifold.

THEOREM 3.2. *Let (M,g), n ≥ 4, be a semi-Riemannian manifold. Then the following three equalities are equivalent :*

$$\sum_{(X_1,X_2)(X_3,X_4)(X,Y)} (R \cdot \widetilde{C})(X_1, X_2, X_3, X_4; X, Y) = 0, \qquad (17)$$

$$\sum_{(X_1,X_2)(X_3,X_4)(X,Y)} (\widetilde{C} \cdot R)(X_1, X_2, X_3, X_4; X, Y) = 0 \qquad (18)$$

and

$$\sum_{(X_1,X_2)(X_3,X_4)(X,Y)} (R \cdot \widetilde{C} - \widetilde{C} \cdot R)(X_1, X_2, X_3, X_4; X, Y) = 0 \qquad (19)$$

on M.

Proof. In view of (10) , we have

$$(R \cdot \widetilde{C})_{hijklm} = g^{rs}(\widetilde{C}_{rijk}R_{shlm} + \widetilde{C}_{hrjk}R_{silm} + \widetilde{C}_{hirk}R_{sjlm} + \widetilde{C}_{hijr}R_{sklm}) \qquad (20)$$

$$(\widetilde{C} \cdot R)_{hijklm} = g^{rs}(R_{rijk}\widetilde{C}_{shlm} + R_{hrjk}\widetilde{C}_{silm} + R_{hirk}\widetilde{C}_{sjlm} + R_{hijr}\widetilde{C}_{sklm}) \qquad (21)$$

Using (9) in (20) we obtain

$$(R \cdot \widetilde{C})_{hijklm} = (R \cdot R)_{hijklm} - \frac{1}{n-2}[g_{ij}(A_{hklm} + A_{khlm}) + g_{hk}(A_{ijlm} + A_{jilm}) - g_{ik}(A_{hjlm} + A_{jhlm}) - g_{hj}(A_{iklm} + A_{kilm})], \qquad (22)$$

where $A_{mijk} = S^r_m R_{rijk}$.
Applying, in the same way, (9) in (21) we get

$$(\widetilde{C} \cdot R)_{hijklm} = (R \cdot R)_{hijklm} - \frac{1}{n-2}[Q(S, R)_{hijklm} + g_{hl}A_{mijk} - g_{hm}A_{lijk} - g_{il}A_{mhjk} + g_{im}A_{lhjk} + g_{jl}A_{mkhi} - g_{jm}A_{lkhi} - g_{kl}A_{mjhi} + g_{km}A_{ljhi}]. \qquad (23)$$

We set

$$\mathcal{F}_{hijklm} = -\frac{1}{n-2}[g_{ij}(A_{hklm} + A_{khlm}) + g_{hk}(A_{ijlm} + A_{jilm}) - g_{ik}(A_{hjlm} + A_{jhlm}) - g_{hj}(A_{iklm} + A_{kilm}) + g_{kl}(A_{mjhi} + A_{jmhi}) + g_{jm}(A_{klhi} + A_{lkhi}) - g_{km}(A_{jlhi} + A_{ljhi}) - g_{jl}(A_{kmhi} + A_{mkhi}) + g_{mh}(A_{lijk} + A_{iljk}) + g_{li}(A_{mhjk} + A_{hmjk}) - g_{mi}(A_{lhjk} + A_{hljk}) - g_{lh}(A_{mijk} + A_{imjk})].$$

Symmetrizing (22) with respect to the pairs (h,i), (j,k) and (l,m) and applying (15) and (16) we obtain

$$\sum_{(X_1,X_2)(X_3,X_4)(X,Y)} (\widetilde{C} \cdot R)(X_1, X_2, X_3, X_4; X, Y) = -\mathcal{F}_{hijklm}$$

In the same way , using (20), we have

$$\sum_{(X_1,X_2)(X_3,X_4)(X,Y)} (R \cdot \widetilde{C})(X_1, X_2, X_3, X_4; X, Y) = \mathcal{F}_{hijklm}$$

From the last two equations we get

$$\sum_{(X_1,X_2)(X_3,X_4)(X,Y)} (R \cdot \widetilde{C} - \widetilde{C} \cdot R)(X_1, X_2, X_3, X_4; X, Y) = 2\,\mathcal{F}_{hijklm}$$

If $\mathcal{F}_{hijklm} = 0$, then (17) (equivalently (18), (19)) holds on M. This completes the proof.

The equations (17) – (19) are named the Walker type identities. We also can consider the following Walker type identity

$$\sum_{(X_1,X_2)(X_3,X_4)(X,Y)} (\widetilde{C}.\widetilde{C})(X_1,X_2,X_3,X_4;X,Y) = 0\,. \qquad (24)$$

THEOREM 3.3. *Let $M(f_1, f_2)$ be an m-dimensional ($m \geq 4$) generalized complex space form. Then we have*

$$\begin{aligned} R.\widetilde{C} - \widetilde{C}.R &= \frac{2}{m-2}[(m-1)f_1 + 3f_2]\,Q(g,R) \\ &= \frac{2}{m-2}[(m-1)f_1 + 3f_2]\,Q(g,\widetilde{C}) \\ &= \frac{2}{m-2}Q(S,R) \\ &= \frac{2}{m-2}Q(S,\widetilde{C}). \qquad (25) \end{aligned}$$

Proof. By using (3) the equations (22), (23) and (9) reduce to

$$R.\widetilde{C} = R.R \qquad (26)$$

$$\widetilde{C}.R = R.R - \frac{2}{m-2}[(m-1)f_1 + 3f_2]\,Q(g,R) \qquad (27)$$

and

$$\widetilde{C} = R - \frac{2}{m-2}[(m-1)f_1 + 3f_2]\,G \qquad (28)$$

respectively. Hence we have

$$R.\widetilde{C} - \widetilde{C}.R = \frac{2}{m-2}[(m-1)f_1 + 3f_2]\,Q(g,R).$$

and so Q (g , R) = Q(g ,$\widetilde{C}$) . This completes the proof.

In view of the above theorem an m-dimensional (m ≥ 4) generalized complex space form satisfying the following conditions:

- the tensors $R.\widetilde{C} - \widetilde{C}.R$ and $Q(g,R)$ are linearly dependent at every point of $M(f_1, f_2)$,
- the tensors $R.\widetilde{C} - \widetilde{C}.R$ and $Q(g,\widetilde{C})$ are linearly dependent at every point of $M(f_1, f_2)$,
- the tensors $R.\widetilde{C} - \widetilde{C}.R$ and $Q(S,R)$ are linearly dependent at every point of $M(f_1, f_2)$,
- the tensors $R.\widetilde{C} - \widetilde{C}.R$ and $Q(S,\widetilde{C})$ are linearly dependent at every point of $M(f_1, f_2)$.

COROLLARY 3.4. *Let $M(f_1, f_2)$, ($m \geq 4$), be an m-dimensional generalized complex space form satisfying $R.\widetilde{C} = 0$, then $M(f_1, f_2)$ is semisymmetric.*

THEOREM 3.4. *Let $M(f_1, f_2)$, be an m-dimensional ($m \geq 4$) generalized complex space form. Then the Walker type identities (17) – (19) and (24) hold on $M(f_1, f_2)$.*

Proof. In view of theorem 3.3., we have

$$R.\widetilde{C} - \widetilde{C}.R = \frac{2}{m-2}[(m-1)f_1 + 3f_2]\,Q(g,R)$$

and using (15) we get (19) (equivalently (17) and (18)).

Further, we note that $\widetilde{C} = R - \frac{2}{m-2}[(m-1)f_1 + 3f_2]\,G$. This gives

$$\begin{aligned} \widetilde{C}.\widetilde{C} &= \widetilde{C}.\left(R - \frac{2}{m-2}[(m-1)f_1 + 3f_2]\,G\right) = \widetilde{C}.R \\ &= \left(R - \frac{2}{m-2}[(m-1)f_1 + 3f_2]\,G\right).R \\ &= R.R - \frac{2}{m-2}[(m-1)f_1 + 3f_2]\,Q(g,R). \end{aligned}$$

Now using (15) and (16) complete the proof.

4. GENERALIZED COMPLEX SPACE FORM SATISFYING R. R – Q(S , R) = L Q(g ,$\widetilde{C}$)

In this section we consider m-dimensional, (m ≥ 4), generalized complex space forms satisfying the condition

$$R.R - Q(S,R) = L\,Q(g,\widetilde{C}) \qquad (29)$$

on $\mathcal{U}_{\widetilde{C}} = \{x \in M(f_1, f_2) \mid \widetilde{C} \neq 0 \text{ at } x\}$, *where L is some function on* $\mathcal{U}_{\widetilde{C}}$.

THEOREM 4.1. *Let $M(f_1, f_2)$ be an m-dimensional ($m \geq 4$) generalized complex space form. If the relation (29) fulfilled on $\mathcal{U}_{\widetilde{C}} \subset M(f_1, f_2)$, then $M(f_1, f_2)$ is pseudo-symmetric with the function $L_R = L + (m-1)f_1 + 3f_2$.*

Proof. Using (3) and (28) in (29), we have

$$R.R - [(m-1)f_1 + 3f_2]\,Q(g,R) = L\,Q(g,\widetilde{C})$$

and so

$$R.R = [L + (m-1)f_1 + 3f_2]\,Q(g,R).$$

This completes the proof.

 ISSN: 2651-5199

ACKNOWLEDGMENT

The author would like to thank the referees for the careful review and their valuable comments.

REFERENCES

[1] Z. Olszak, "The existance of generalized complex space form", Israel.J.Math., vol.65, pp.214- 218, 1989.
[2] U.C. De and A. Sarkar,"On the projective curvature tensor of generalized Sasakian space forms", Quaestines Mathematicae, vol.33, pp.245-252, 2010.
[3] Sarkar. A. and De. U.C, "Some curvature properties of generalized Sasakian space forms", Lobachevskii journal of mathematics, Vol.33, no.1, pp.22-27, 2012.
[4] Venkatesha and B. Sumangala, "On M-Projective curvature tensor of a generalized Sasakian space form", Acta Math. Univ. Comenian, Vol.82(2) pp.209-217, 2013.
[5] M. Atceken , "On generalized Saskian space forms satisfying certain conditions on the concircular curvature tensor", Bulletin of Mathemaical analysis and applications, vol.6(1), pp.1-8, 2014.
[6] S. Yadav, D.L. Suthar and A. K. Srivastava , "Some results on M(f_1, f_2, f_3) 2n+1-manifolds", Int. J. Pure Appl. Math., vol.70(3), pp.415-423, 2011.
[7] H. G. Nagaraja and Savithri Shashidhar, "On generalized Sasakian space forms", International Scholarly Research Network Geometry, 2012.
[8] M. C. Bharathi and C. S. Bagewadi, "On generalized complex space forms", IOSR Journal of Mathematics, vol.10, pp. 44-46, 2014.
[9] K. Yano, *Differential geometry on complex and almost complex spaces*, Pergamon Press, 1965.
[10] F. Tricerri and L. Vanhecke "Curvature tensors on almost Hermitian manifolds", Trans. Amer. Math. Soc., vol. 267, pp.365-398, 1981.
[11] U.C. De and G.C. Ghosh "On generalized Quasi-Einstein manifolds" Kyungpoole Math.J., vol.44, pp. 607-615, 2004.
[12] Z.I. Szabó, "Structure theorems on Riemannian spaces satisfying R(X,Y).R=0", I. The local version, J. Differential Geom., vol.17, pp.531-582, 1982.
[13] R. Deszcz, "On pseudosymmetric spaces", Bull. Soc. Math. Belg. Ser., Vol. A44, pp.1-34, 1992.
[14] R. Deszcz and Ş. Yaprak, "Curvature properties of certain pseudosymmetric manifolds",Publ. Math. Debr., vol.45, pp.334-345, 1994.
[15] R. Deszcz and M. Hotlos , "Remarks on Riemannian manifolds satisfying a certain curvature condition imposed on the Ricci tensor", Prace. Nauk. Pol. Szczec., vol. 11, pp. 23-34, 1989.
[16] M. Belkhelfa, R. Deszcz, M, Głogowska, M. Hotlos, D. Kowalczyk and L. Verstraelen, " A Review on pseudosymmetry type manifolds", Banach Center Publ., vol.57, pp. 179-194, 2002.
[17] R. Deszcz, J. Deprez and L. Verstraelen, "Examples of pseudo-symmetric conformally flat warped products", Chinese J. Math., vol. 17, pp.51-65, 1989.

Kinetic Investigation of Boronized 34CrAlNi7 Nitriding Steel

Polat TOPUZ, Tuna AYDOĞMUŞ, Özlem AYDIN

Machinery and Metal Technology Department, İstanbul Gedik University
Istanbul, Turkey
polat.topuz@gedik.edu.tr; tuna.aydogmus@gedik.edu.tr; ozlem.aydin@gedik.edu.tr

Abstract: In this study, kinetic examinations of boronized 34CrAlNi7 Nitriding Steel samples were described. Samples were boronized in indirect heated fluidized bed furnace consists of Ekabor 1™ boronizing agent at 1123, 1223 and 1323 K for 1, 2 and 4 hours. Morphologically and kinetic examinations of borides formed on the surface of steel samples were studied by optical microscope, scanning electron microscope (SEM) and X-Ray diffraction (XRD). Boride layer thicknesses formed on the steel 34CrAlNi7 ranges from 46,6 ± 3,8 to 351,8 ± 15,2 μm. The hardness of the boride layer formed on the steel 34CrAlNi7 varied between 1001 and 2896 kg/mm^2. Layer growth kinetics were analyzed by measuring the extent of penetration of FeB and Fe_2B sublayers as a function of boronizing time and temperature. The kinetics of the reaction has been determined with K=Ko exp (-Q/RT) equation. Activation energy (Q) of boronized steel 34CrAlNi7 was determined as 169 kj/mol.

Keywords: Boronizing, 34CrAlNi7, Indirect Heated Fluidized Bed Furnace, Kinetics of Boron.

1. INTRODUCTION

Boron element in the periodic table is located next to the carbon. The boron and its compounds are in a unique position in terms of their properties in various applications [1]. In the periodic table, the boron, indicated by the symbol *B*, is a semiconductor element with an atomic weight of 10,81 and an atomic number of 5 and it is also the first and the lightest element of group 3A in the periodic table. Metallic or non-metallic elements produced from boron compounds have wide use in the industry. Under normal conditions, boron compounds have the property of non-metal compound, but pure boron, like carbon element, has electrical conductivity. In addition, the crystalline boron has similar properties to the diamond. For example, its hardness is close to diamond [2].

Boronizing, also commonly referred to as boriding, is a thermochemical surface hardening process applied to well cleaned surfaces of metallic materials at high temperatures. As a rule, Boronizing treatments are usually carried out between 1123 and 1223 K. The boride layers formed as a result of boronizing treatment have high hardness as well as wear, corrosion and high heat resistance [3]. Boronizing increases the resistance to certain acid types, partly to hydrochloric acid. It is possible that the irregularly shaped parts can be boronized evenly and have a positive effect on the tool life [4]. The formation of boride layer is diffusion controlled. As the temperature increases, the thickness of the boride layer formed on boronized iron surfaces also increases. The phase formed as a result of boriding of iron-based materials, only FeB, is the permanent tension, prone to tensile, if the phase, Fe_2B, is prone to compress. Because of this situation, the phases apply the tensile-compressive force in the double-phase boride layers [5,6]. The hardness depends on the type of material and FeB or Fe_2B phases on the surface. FeB phase is harder and brighter than Fe_2B phase [7]. The atoms of the boronizing compound used in the boronizing process are settled between the atoms of the iron-based material by diffusion. The hardness of the boride layer changes depending on the composition of the boronized material and the structure of the boride layer [8].

One of the methods used for the boronizing process is the *pack boronizing* technique. This technique is based on the principle of heating the material embedded in the boron powder mixture in a heat-resistant steel pot by the furnace [9]. There are many powder mixtures for boronizing in the literature. But the common point of all is the formation of boron source, activator and inert diluents. The Ekabor boronizing agent used in this study is also a powder mixture containing these components. It is stated that in the literature, this boronizing agent is composed of 5% B_4C + 5% KBF_4 + 90% SiC [8,10].

As boronizing is widely used in different engineering areas and industrial sectors. Some of these sectors can be listed as follows; metallurgy and materials, mining, textile, chemical and mechanical engineering and also agriculture, food and porcelain industry [11].

Boriding can be carried out on different types of cast irons and steels such as structural steels, case hardened steels, tool steels, stainless steels, cast steels, or sintered steels. However, due to the risk of cracking between FeB and Fe_2B phases in nitriding steels, a thick layer of boride is not desirable [12].

In this study, the activation energy (Q) value required for boronizing of 34CrAlNi7 nitriding steel and the growth rate constant of boride layer were investigated. Arrhenius equation was used to determine the relationship between growth rate constant and activation energy [13].

2. MATERIAL AND METHOD

In this study, 34CrAlNi7 nitriding steel material was boronized. The results of the chemical analysis performed with optical emission spectrometry prior to the experimental procedures are shown in Table 1. below.

Table 1. The chemical composition of 34CrAlNi7

Boronized Material	Alloying Elements (wt.-%)				
	C	Mn	Si	Cr	Ni
34CrAlNi7 Nitriding Steel	0,38	0,72	0,23	1,66	0,80
	Alloying Elements (wt.-%)				
	Mo	V	W	Al	
	0,17	0,03	0,04	0,98	

The pack-boronizing method was used for the boronizing heat treatment. In this method, commercial name is Ekabor 1™ powder mixture was used. Samples embedded in Ekabor 1™ powder in AISI 304 stainless steel pot were heated in fluidized bed furnace at 1123, 1223 and 1323 K as three process temperatures and for 1h, 2h and 4h as three different treatment times. Then the boronized samples were cooled in air. After this processes, boronized samples were sanded with 120 to 1000 numbered emery paper, then polished with diamond paste. The free from scratches samples were etched by Nital 4 (4% HNO_3 + 96% ethyl alcohol) etcher. An optical microscope and an integrated image analyzer were used to measure the thickness of the boron layer formed on the surface of the samples. In order to obtain a more detailed view of the two-phase boride layer, a SEM image of the sample was taken with the help of the back scattered electrons. The microstructural studies were carried out on boronized samples. Vickers hardness tester was used for hardness measurements. The hardness measurements were performed from surface to matrix, by 4 different points and using with 100 g. weight.

3 RESULT AND DISCUSSION

3.1. Microstructure and Hardness Analyses

It has been revealed in many studies [8, 10, 13] that the boron layer formed on stainless steels has a columnar morphology. On the contrary, in this study, the shape of the boron layer formed by the saw-tooth morphology also shown in Figures 1, 2 and 3. In addition to the binary phase structure forming the boride layer and the matrix microstructures are also shown in Figure 4.

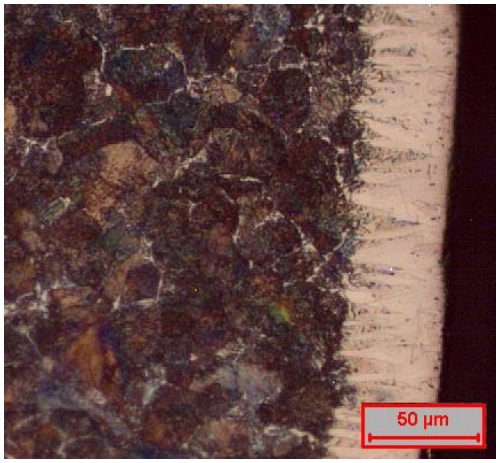

1h.

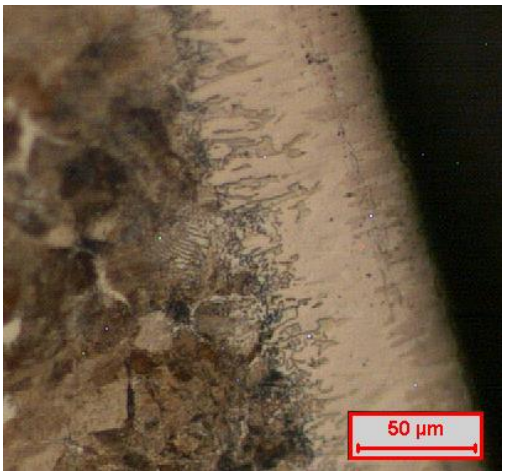

2h.

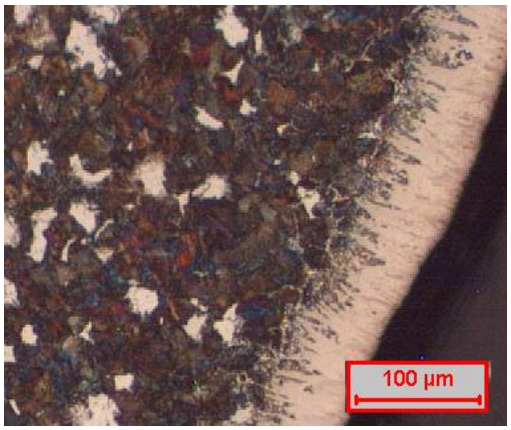

3h.

Figure 1. Boride layers formed on 34CrAlNi7 at 1123 K

ISSN: 2651-5199

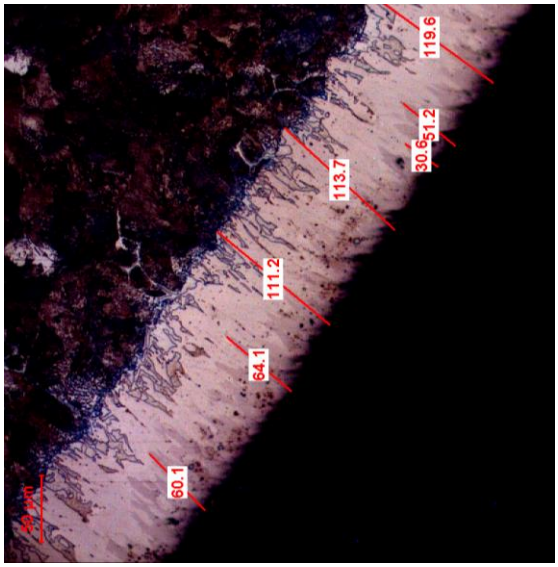

1h.

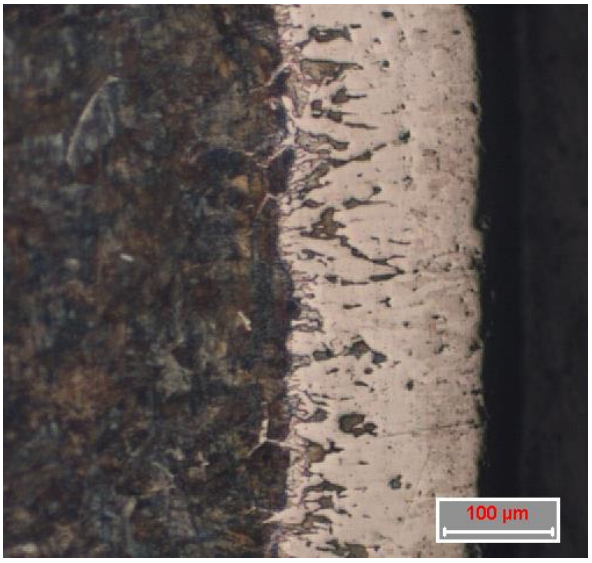

1h.

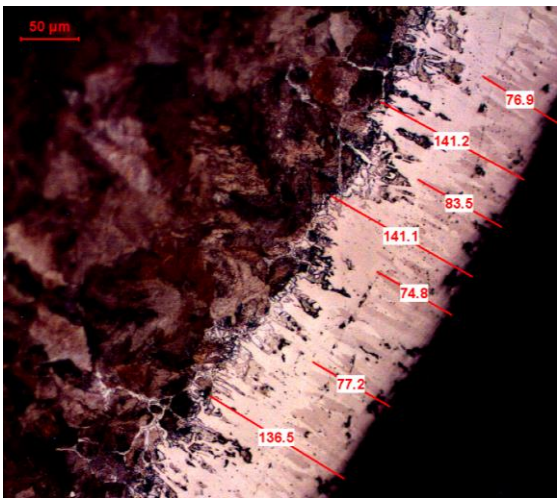

2h.

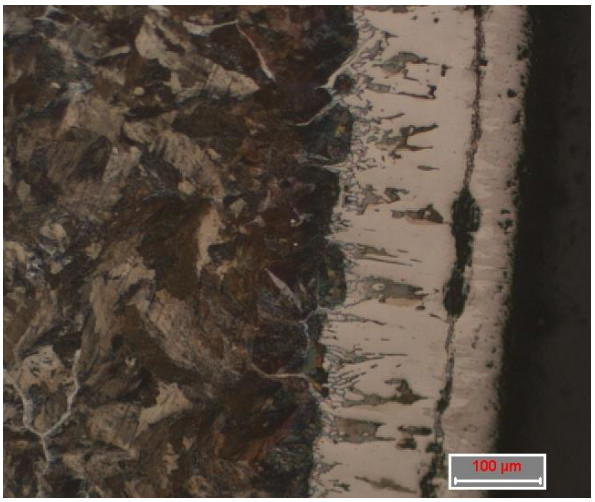

2h.

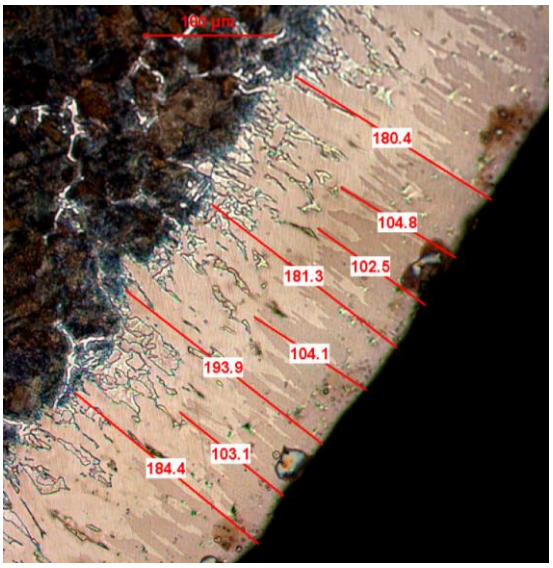

3h.

Figure 2. Boride layers formed on 34CrAlNi7 at 1223 K

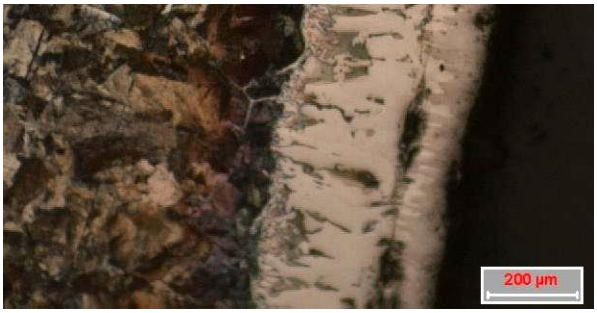

3h.

Figure 3. Boride layers formed on 34CrAlNi7 at 1323 K

According to the microstructure investigations, boride layer formed on the surface of the boronized 34CrAlNi7 nitriding steel was found to consist of FeB and Fe_2B phases. As can be seen from the SEM (BEI) image, the outermost dark gray phase is FeB and the adjacent light gray color phase is Fe_2B.

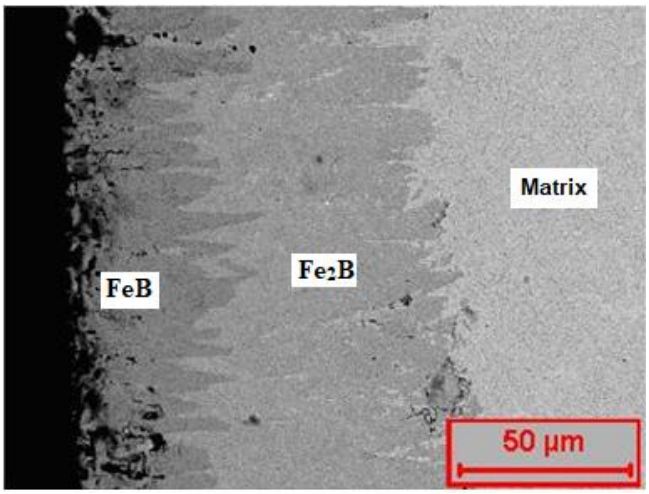

Figure 4. SEM (BE) image of boronized 34CrAlNi7

In the present investigation, the boride layer thicknesses of the boronized samples at three different temperatures and times range from 42,8 to 367µm. Measurement results of the layer thicknesses can be seen from Figure 3. as well as Table 2.

.

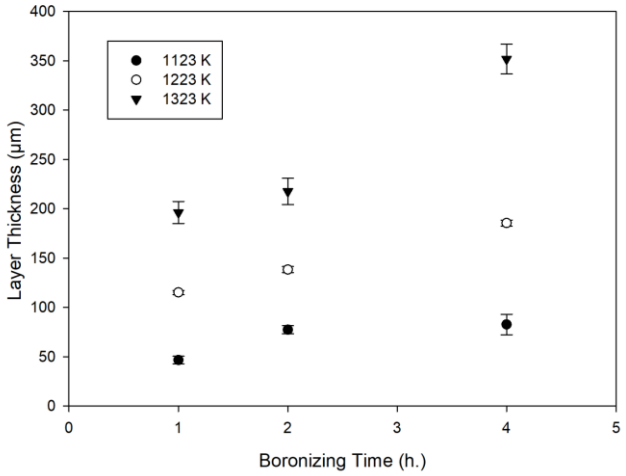

Figure 5. Thicknesses of boride layer on 34CrAlNi7

Table 2. Boride layer thicknesses on 34CrAlNi7

Boronized Material	Boronizing Temperature (K)	Boronizing Time (hour)	Boron Phase Layer Thickness (µm)
34CrAlNi7	1123	1	46,6±3,8
		2	77,3±4,1
		4	82,6±10,4
	1223	1	115,2±2,1
		2	138,4±3,1
		4	185,5±2,1
	1323	1	196,3±11,2
		2	217,6±13,3
		4	351,8±15,2

The hardness values measured from the surface to the matrix by the Vickers method at a distance of 20 µm to 220 µm and the changes in these values can be seen at Table 3.

Table 3. Microhardness measurements of the boronized 34CrAlNi7

Boronizing Temp. (K)	Boronizing Time (h.)	Microhardness Measurement (kg/mm^2) Distances From Surface to Center			
		20µm	40µm	100µm	220µm
1123	4	2216	1961	426	381
	2	2106	1899	389	317
	1	1869	971	361	321
1223	4	2857	2446	2016	392
	2	2814	2167	1896	321
	1	2321	2002	1772	383
1323	4	2896	2521	2111	1997
	2	2881	2186	1989	1808
	1	2403	1999	1921	1001

3.2 XRD Analyses

XRD analyses were carried out on the sample that had been boronized for 1123K, 1223K and 1323K for 1 h. For analysis, Philips Panalytical X-Pert Pro Brand X-Ray Diffractometer is used. Cu(Kα) having the wavelength 1.5406 Å which matches the interatomic distance of crystalline solid materials as well as the intensity of Cu(Kα) is higher than other which is sufficient for the diffraction of solid material so Cu(Kα) is used for analysis. The peaks obtained after the analysis are shown in Figure 3.

As in all steel types, boride layer formed on 34CrAlNi7 has a double-phase structure occure with FeB and Fe_2B. However, due to the alloying elements in this type steel, small amounts of Fe_3B, FeB_{49}, Cr_2B and Cr_5B_3 phases were found.

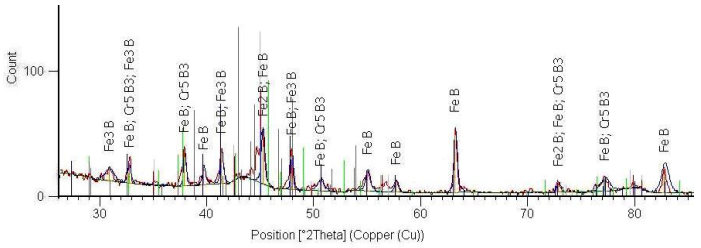

(a)

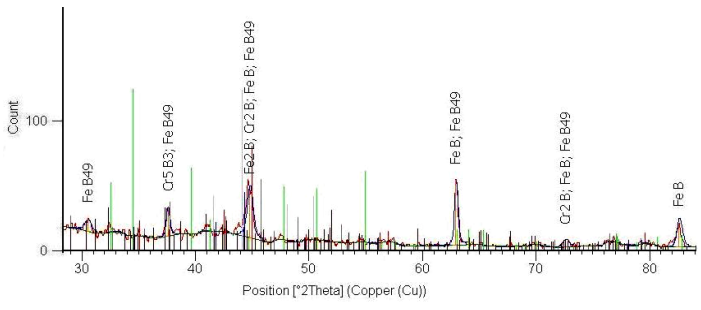

(b)

ISSN: 2651-5199

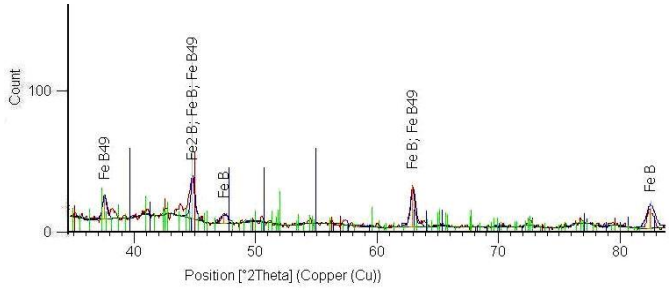

(c)

Figure 5. X-ray diffraction patterns of boronized 34CrAlNi7 (1h.) at different temperatures, a)1123K, b)1223K, c)1323K

3.3 Kinetic Examinations

The equation that determines the thickness of boride layer changes parabolically over time is given below [8,13].

$$x = \sqrt{Kt} \quad (1)$$

According to this equation; *x* indicates the boride layer thickness in cm, *t* indicates the boronizing time in s., and *K* indicates the growth rate constant in $cm^2\ s^{-1}$. If the growth kinetics of the boride layer is desired; As can be seen from Figure 4, the square of the boride layer thickness changes linearly over time.

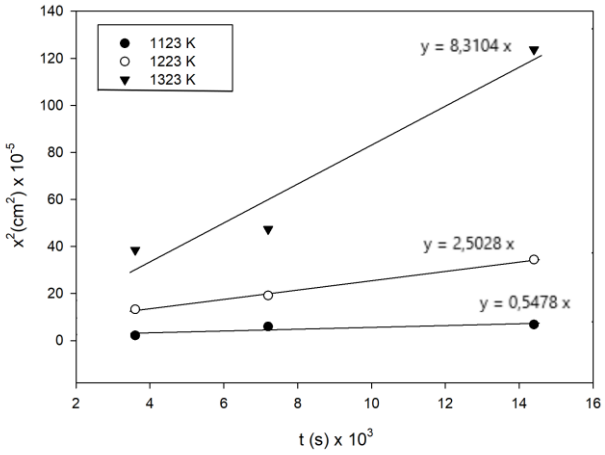

Figure 6. Square of the boride layer thicknesses on boronized steel 34CrAlNi7over treatment time.

Boron diffusion is the primary factor affecting layer growth. The relationship between growth rate constant and activation energy is explained by the Arrhenius equation is given below [13,14].

$$K = K_0 \times \exp\left(-\frac{Q}{RT}\right) \quad (2)$$

According to equation; *K* indicates the growth rate constant in $m^2\ s^{-1}$, *Q* indicates the activation energy in j mol^{-1}, K_0 indicates the pre-exponential constant in $m^2\ s^{-1}$ and *R* indicates the gas constant in j $mol^{-1}\ K^{-1}$. Equation 3 is natural logarithm of Equation 2.

$$\ln(K) = \ln(K_0) - \left(\frac{Q}{RT}\right) \quad (3)$$

In order to find the activation energy value, ln K - 1 / T graph should be plot first. The slope of this graph gives the activation energy value and this can be seen in Figure 7.

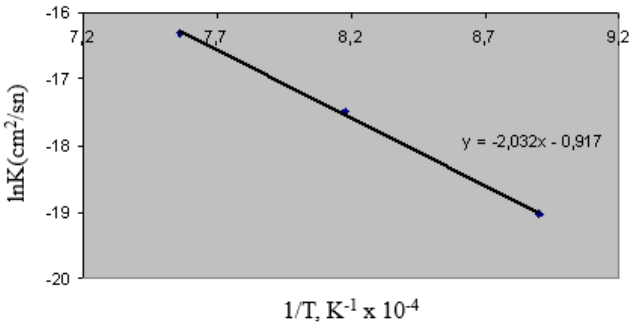

Figure 7. Growth rate constant vs. temperature of boronized 34CrAlNi7

The activation energy and pre-exponential constant values were obtained from the relationship of the slope of the straight line obtained at 1 / T = 0 with the abscissa as origin; the results are listed in Table 4.

Table 4. Activation energy, frequency factor, and diffusion depth of boronized 34CrAlNi7

Boronized Material	**Q (kj/mol)**	**K_0**
34CrAlNi7	169	$40*10^{-2}$
	x (cm)	
	$\sqrt{40*10^{-2} \exp(20320/T) * t}$	

3.4 Discussion

Based on these experimental results, boride layer can be formed on the 34CrAlNi7 nitriding steel surface without oxidation with fluidized bed furnace by pack boronizing treatment. At the same time, it is an efficient way to obtain high surface hardness. Increasing treatment time and temperature, increases layer thickness.

The microstructures showed that two distinct regions were identified on the surface of the specimens; the boride layer formed from FeB and Fe_2B phases, and matrix. Unlike the stainless steels, the boride layer formed on 34CrAlNi7 has a saw-tooth morphology.

From the micro hardness measurements, a decrease in hardness values from the surface to the matrix was found. This is because, the amount of boron in the Fe_2B phase is less than in that FeB phase.

According to the XRD results, boride layer formed on 34CrAlNi7, has a double-phase structure occure with FeB and Fe_2B. However, due to the other alloying elements in this type of steel, Fe_3B, FeB_{49}, Cr_2B and Cr_5B_3 phases were also found. The Arrhenius equation was used to calculate the growth kinetics of the boride layer. As a result of calculations, activation energy of boronized 34CrAlNi7 nitriding steel has been determined as 169 kJ/mol. and this value is consistent with the other studies in the literature. This comparison can be seen in Table 5.

Table 5. The comparison of activation energy for diffusion of boron with respect to the different studies

Type of steel	Range of Temp. (K)	Boronizing Process	Activation Energy (kj/mol)	Ref.
34CrAlNi7	1123-1223	Powder pack	270	[15]
	1123-1323	Powder pack	169	This study
X5CrNi 18-10	1123-1323	Powder pack	244	[16]
X5CrNi 18-10	1123-1223	Powder pack	234	[17]

REFERENCES

[1] Narayan S. Hosmane, Boron Science: New Technologies and Applications, 1st ed., Boca Raton, New York, USA: CRC Press, Taylor & Francis Group, 2011, pp.1.

[2] http://www.boren.gov.tr/en/boron/boron-element, (date of access:24.8.2018)

[3] Joseph R. Davis, Surface Hardening of Steels: Understanding the Basics, 1st ed., Materials Park, OH, USA: ASM International, 2002, pp.213-216.

[4] P.Topuz, E.Yılmaz and E.Gündoğdu, "Kinetic Investigations of Boronized Cold Work Tool Steels", Materials Testing, Vol. 56, no. 2, pp.104-110, 2014.

[5] X. Dong, J. Hu, Z. Huang, H. Wang, R. Gao, Z. Guo,"Microstructure and Properties of Boronizing Layer of Fe-based Powder Metallurgy Compacts Prepared by Boronizing and Sintering Simultaneously" Science of Sintering, V.41, pp.199-207, 2009, doi: 10.2298/SOS0902199D

[6] M.O. Domínguez, M. A. F Renteria, M. Keddam, M. E. Espinosa, O. D. Mejia, J. I. A. Gonzalez, J. Z. Silva, S. A. M. Moreno, J. G. G. Reyes. "Simulation of growth kinetics of Fe_2B layers formed on gray cast iron during the powder-pack boriding" MTAEC9, 48/6, 905, 2014

[7] B. M. CARUTA. Thin Films and Coatings: New Research, p.158, Nova Publishers, 2005

[8] Sinha AK., Boriding (Boronizing) in ASM Handbook, Vol 4: Heat Treating. 1st ed., Materials Park, OH, USA: ASM International, 1991, pp.978-983

[9] Patric Jacquot, Advanced Techniques for Surface Engineering – Nitriding, Boriding and Carburizing of Steels, 1st ed., Kluwer Academic Publishers, Dordrecht, The Netherlands, 1992, pp.76.

[10] Iswadi J.,Yusof H.A.M., Rozali S. and Ogiyama H., "Effect of powder particle sizes on the development of ultra and surface through superplastic boronizing of duplex stainless steel" Journal of Solid Mechanics and Materials Engineering. Vol. 1, pp.539-546, 2007.

[11] Krukovich M.G., Prusakov B.A. and Sizov I.G. The Use of Boriding Processes in the Industrial Treatment of Details and Tools in Plasticity of Boronized Layers. Springer Series in Materials Science, vol 237, Springer, Cham., pp. 301-302, 2016.

[12] http://surface-heat.com/boronizing (date of access 2019)

[13] O. Özdemir, M. A.Omar, M. Usta, S. Zeytin, C.Bindal and A.H. Ucisik, " An investigation on boriding kinetics of AISI 316 stainless steel", Vacuum, Vol.83, pp.175-179, 2008.

[14] Fernandes, F. A. P., Heck, S. C., Totten, G. E. and Casteletti, L. C., "Wear Evaluation of PackBoronized AISI 1060 Steel", *Materials Performance and Characterization*, Vol. 2, No. 1, pp. 58–66, 2013.

[15] Efe,G.Ç.; İpek,M.; Özbek,İ.; Bindal.C: "Kinetics of Borided 31CrMoV9 and 34CrAlNi7 Steels" Materials Characterization 59, 23 – 31 (2008)

[16] P. Topuz, B. Çiçek, O. Akar: "Kinetic Investigation of AISI 304 Stainless Steel Boronized in Indirect Heated Fluidized Bed Furnace" *Journal of Mining and Metallurgy*, Section B: Metallurgy, Vol.52 No.(1) B, pp. 63 – 68, 2016

[17] Kayalı, Y., "Investigation of the Diffusion Kinetics of Borided Stainless Steel"s, *The Physics of Metals and Metallography*, Vol. 114 (12), pp.1061–1068, 2013.

 ISSN: 2651-5199

İstanbul
GEDİK
University
2651-5199